Original Article - Special issue 75th ABM Annual Congress

Characterization of first generation advanced high strength steel of the complex phase class for automotive application though light optical microscopy and electron backscattering diffraction

Renan de Melo Correia Lima [1]*
Julio Cesar Spadotto [2]
Flavia Tereza dos Santos Tolomelli [3]
Fernando Cosme Rizzo Assunção [1]

Abstract

As the demand for Advanced High Strength Steels (AHSS) increases, the need for faster and reliable ways to identify their microstructure and quantify the phase distribution becomes more evident. For some types of steels this can be done by a simple color etching and light optical microscopy (LOM) imaging. On the other hand, steels with more complex microstructural distribution require a combination of additional techniques, many of which are time-consuming, such as dilatometry or electron backscattering diffraction (EBSD). In this work, a combination of LOM and EBSD was used to quantify the microstructure of Complex-Phase steels. The methods used to process the data and distinguish the microconstituents in EBSD is explained and some exemplary results obtained in industrial steels are reported. Also, a previously used way to quantitatively compare the LOM and EBSD results is also shown to confirm the validity of the approach discussed in the present work.

Keywords: Microstructural characterization; Complex-Phase AHSS steel; EBSD.

1 Introduction

Complex-phase (CP) steels are part of the first generation of Advanced High Strength Steels (AHSS), which are strong and tough, with high yielding strength levels but still presenting a continuous yielding effect [1,2]. Their properties are, in part, due to the combination of the soft, recrystallized ferrite, hard martensite, and bainite as an intermediary microconstituent. In some cases, CP steels also contain retained austenite and even pearlite [1-5]. This kind of steel is mainly used as an alternative for Dual-Phase steels, which present less work flangeability and are more prone to void nucleation [6].

CP steels can be produced by hot-rolling, for lower Ultimate Tensile Strength (UTS) requirements, or via hot-rolling followed by cold-rolling plus an intercritical heat treatment, whenever a higher UTS is required [1]. The heat treatment consists of heating the steel to the intercritical temperature (between A_C1 and A_C3), where a combination of austenite and recrystallized ferrite will be produced. Then, the steel is cooled to a holding temperature where bainite is formed. During the cooling ferrite may be allowed to grow, depending on the cooling rate and the steel composition. After some time of holding in a specific temperature, the steel is quenched to room temperature, forming some martensite. In addition, after such heat treatment a small amount of retained austenite can remain in the material [7].

Phase identification and quantification of a steel constituted by four or more microconstituents is a challenge. Some researchers have applied the combination of color etching and LOM to varying degrees of success [8], and in some cases finding contradictory results [9]. Hairer et al. [8] have studied five different kinds of etching, in which the authors concluded that a combination of grain boundary etching with Nital solution followed by an anodic surface etching with $Na_2S_2O_5$ solution provided the best results. Even then, some contradictory results, based on the color of each microconstituent in steels can be found in the literature [1].

Another more recent alternative for phases identification in steels is the EBSD technique. Garcia et al. [10] have reported on the increase of dislocation density in microconstituents formed in lower temperatures, as well as, how this higher dislocation density affect the quality of the Kikuchi patterns generated during the EBSD analysis. From the EBSD analysis, the quality of the patterns can be seen in a grayscale map, and a deconvolution of the grayscale histogram can be used to

[1]*Departamento de Química e Engenharia dos Materiais, DEQM, Pontificia Universidade Católica do Rio de Janeiro, PUC-Rio, Rio de Janeiro, RJ, Brasil.*
[2]*Department of Materials, Henry Royce Institute, The University of Manchester, Manchester, United Kingdom.*
[3]*Departamento de Engenharia e Ciência dos Materiais, Instituto Militar de Engenharia, IME, Rio de Janeiro, RJ, Brasil.*

**Corresponding author: renanmeloclima@gmail.com*

Table 1. Chemical composition of steel (wt.%) [14]

C	Mn	Si	Cr	Al	Nb
<0.17	>1.6	0.2	>0.2	>0.015	>0.01

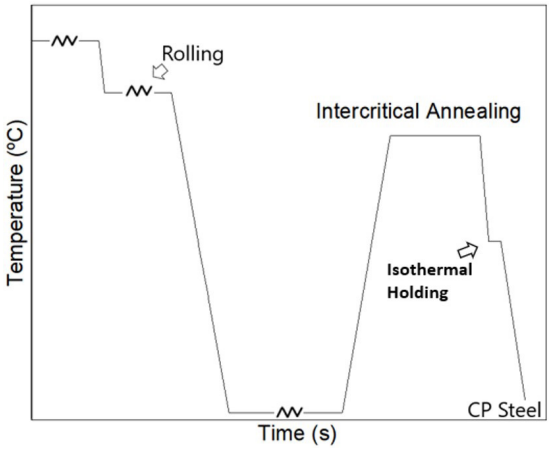

Figure 1. Schematic design of the CP steel treatment.

differentiate the microconstituents in steels [10-13]. To improve the phase identification in steels with complex microstructure it is recommended the combination of this grayscale map with the Kernel Average Misorientation (KAM) and the Grain Orientation Spread (GOS) maps. These maps (KAM and GOS) provide a measurement of how much the grain deviate from its average angle. The use of this combination applied in steels has been reported by several authors [12,14,15].

In this work, a combination of LOM and EBSD was used to identify and quantify the microstructure of a CP1100 steel. This steel had been previously characterized and the influence of its microstructure on the mechanical properties discussed. Here, a more comprehensive, step by step, explanation of the characterization procedure is presented as a basis for future work.

2 Material and methods

An industrially produced, low silicon, low manganese, niobium alloyed steel was used in the present work. The approximated chemical composition of the steel is shown in Table 1. As indicated by the mechanical properties in Table 2, this is a high strength CP1100 steel.

As mentioned before, the production of a CP steel includes a hot rolling step, a cold rolling step and an intercritical annealing, followed by an isothermal holding. During an industrial processing, a galvanizing step needs to be applied as well. Figure 1 displays a schematic design of the full CP treatment.

2.1 Sample preparation

Metallographic samples for LOM analysis were manually prepared by grinding with SiC paper FEPA designated P400, P600, P800, and P1200 followed by polishing with diamond suspensions of 9, 6, 3, 1 and 0.25 µm. The samples were then etched using 2% Nital followed by 1% sodium metabisulphite solution. Under bright field LOM imaging, these etching reveals ferrite as white, bainite/martensite as brown and retained austenite as black regions [8,16]. Although there are some small variations in the brown regions that could be used to differentiate between bainite and martensite, the distinction is neither easily made nor reproductible, attempts to quantify such microconstituents lead to more than 10% of deviation in the results.

Table 2. Mechanical properties of the CP1100 steel [14]

YS(MPa)	UTS(MPa)	El. (%)
831	1112	9

The EBSD samples were the same used for the LOM characterization, therefore, the samples were already etched. However, these samples were polished with using 1 and 0.25 µm diamond suspensions. Following, a final polishing was done in a Minimet®1000, using colloidal silica MasterMet2® solution (0.02 µm). The polishing time in the Minimet varied between 3 and 5 hours.

2.2 LOM imaging processing

No image processing was applied to the LOM images prior to the segmentation. Segmentation is a process to distinguish different elements of an image. In this case, the elements are the different microconstituents.

Preprocessing the image with contrast modification can make easier for a human user to identify the constituents, but it may negatively impact the automatic segmentation method used. The segmentation was performed in the FIJI open-source software, using the Waikato Environment for Knowledge Analysis (WEKA) plugin [17]. This plugin is used to train a neural network that does the segmentation. The process is done by manually selecting grain from each phase. The software will consider information such as the color value of the selected grain, the difference of the gaussian distribution in several regions, the value of the neighbors, among other options. The selected characteristic for this quantification were: Gaussian Blur; Hessian; Membrane Projections; Sobel filter; Difference of gaussians; and Neighbors. A more comprehensive explanation of the method and the mathematics behind the filter can be found in the developer's publication and its web page [17]. An example of this segmentation is seen in Figure 2.

2.3 EBSD maps and post-processing

From the EBSD analysis of the CP steels, five different kinds of maps were used in this investigation. They are:

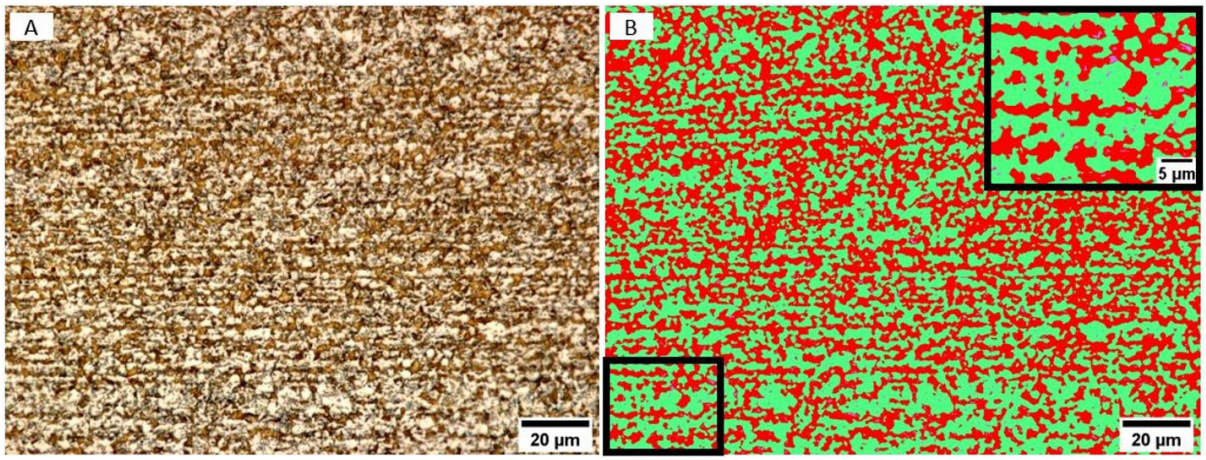

Figure 2. Segmentation of CP steel using WEKA. A – LOM image prior to segmentation, whitish ferrite, brown martensite/bainite, black retained austenite. B – Segmented image, green ferrite, red martensite/bainite, purple retained austenite. The insert in B shows a region containing retained austenite. Reproduced from Lima et al. [14].

- Band Contrast (BC), derived from the Hough transformation, that provides contrast from the average intensity of the Kikuchi pattern in pixels, regarding to the overall pattern quality. This map was used to determine if there is any residual deformation from the sample preparation that may affect the phase segmentation. In CP steels characterization is also used to segment the martensite, since its highly deformed crystal structure is not properly identified, making it a zero solution (not identified) or a ferrite identification.
- Phase Map, segment regions based on the crystallographic structure of each crystal. In this work, it was used to distinguish the retained austenite from the other phases.
- Inverse Pole Figure (IPF) shows the crystallographic orientation of each crystal in a given axis. It is used to look for preferential orientation and texture in the steel.
- Kernel Average Misorientation (KAM), it is a local deviation map that measures the deviation of a pixel in relation to a small kernel of neighbors. Regions with high dislocation density (deformed regions) will present high values of KAM and it will be highlighted in this map. In the present work, KAM map was used in the machine learning process for the microconstituents segmentation.
- Grain Orientation Spread (GOS), shows the average orientation deviation within one specific grain, that is, how much the orientation changes in a single grain. The bainite regions in the EBSD are not identified sheave by sheave, they are segmented as big bainitic regions. These regions present higher deviation angles than ferrite, making this GOS map appropriated for the microconstituent segmentation between ferrite and bainite.

The post-processing and segmentation were done using the Aztec Crystal® software [18]. The first step during the segmentation is to identify properly the grain to prevent misidentification. When grains are not properly separated, they will form a large region with high GOS, this is likely to lead to an incorrect bainite identification. Figure 3 shows an example of an unsuccessful grain identification. In Figure 3A, the two grains highlighted by the white line were identified as one grain. On the other hand, after applying a lower grain boundary angle it was possible to separate both grains, as shown in Figure 3B.

Following the grain separation, the data is cleaned. This process is done using the "*exclude void based on band contrast*" option, followed by a "*remove zero solution*" with three neighbor's algorithms. Then, the reclassifying tool was used for the microconstituents segmentation. This classification is performed by a machine learning process. This process is a more refined segmentation, when compared to the neural network in the WEKA, and it is a proprietary information from Oxford™. Nevertheless, it is more reliable for repetitive process. For this step of the segmentation, BC, KAM and GOS maps were used overlapping each other. Retained austenite was set as a protected phase in the Aztec Crystal software, which means that this phase will be segmented based on the phase map and the pixels that are identified as such do not go through the machine learning process. The combination of KAM and GOS maps produces a map with regions that have high orientation deviations being highlighted. Those deviations are considered deformed regions and they are identified as the bainite microconstituent.

This segmentation process is highly sensitive to local deformation on the material surface, which makes the sample preparation the most important step for the EBSD characterization prior to any analysis [10,18-21]. Surface scratches, even if polished out, may leave deformation which has influence in the quality of the diffraction patterns obtained during the EBSD analysis. As a consequence, such

deformation will affect the segmentation. Figure 4 shows an example of incorrect segmentation due to residual deformation.

BC map in Figure 4A shows the microstructure of a Ferritic-Bainitic (FB) steel where it is clear the existence of two scratches in this region of the sample. The scratch on the top right corner introduced a misidentification of grains following the direction of such scratch, as indicated in Figure 4B.

This example in Figure 4 shows, first, how the misinterpretation of the results can happen if the sample is not properly prepared and, second, how important it is to always look to the band contrast together with the segmented map. If only the map of Figure 4B was observed, it would be difficult to notice the segmentation problem.

3 Results

A series of LOM imagens were obtained, segmented, and quantified. The results are shown in Table 3.

Figure 5 shows an example of the segmentation process using EBSD for a CP steel. BC map in Figure 5A confirms no residual deformation due to the sample preparation. IPF map (Figure 5B) presents a small {111} orientation preference, with texture index of 3.1. The combination of KAM and GOS maps can be seen in Figure 5C, where deformed regions is shown in green and red (inset in this figure).

Figure 5D presents the segmented map, where red was identified as ferrite, green as bainite, black as martensite,

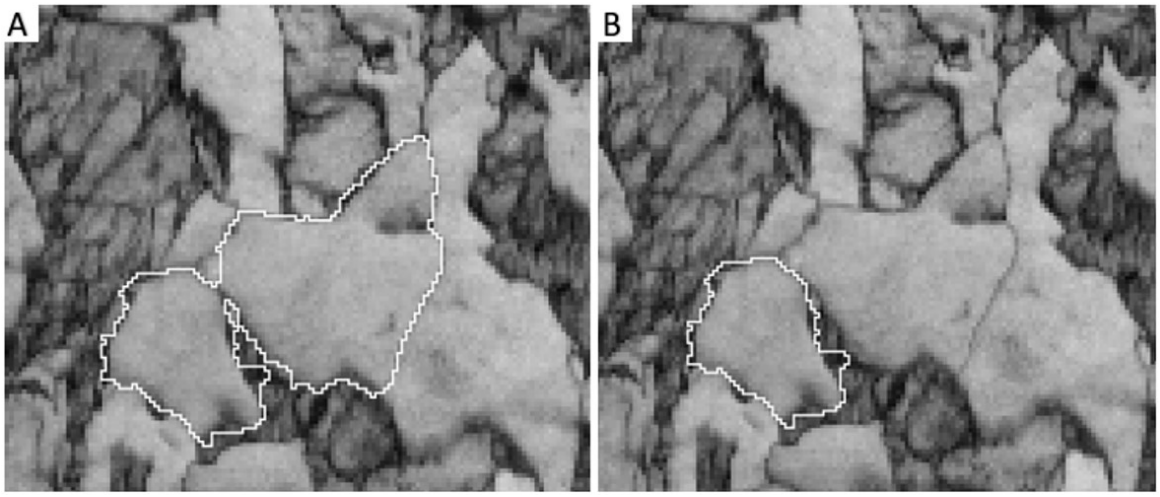

Figure 3. Example of a grain misidentification. A – Incorrect identification. B – Correct identification.

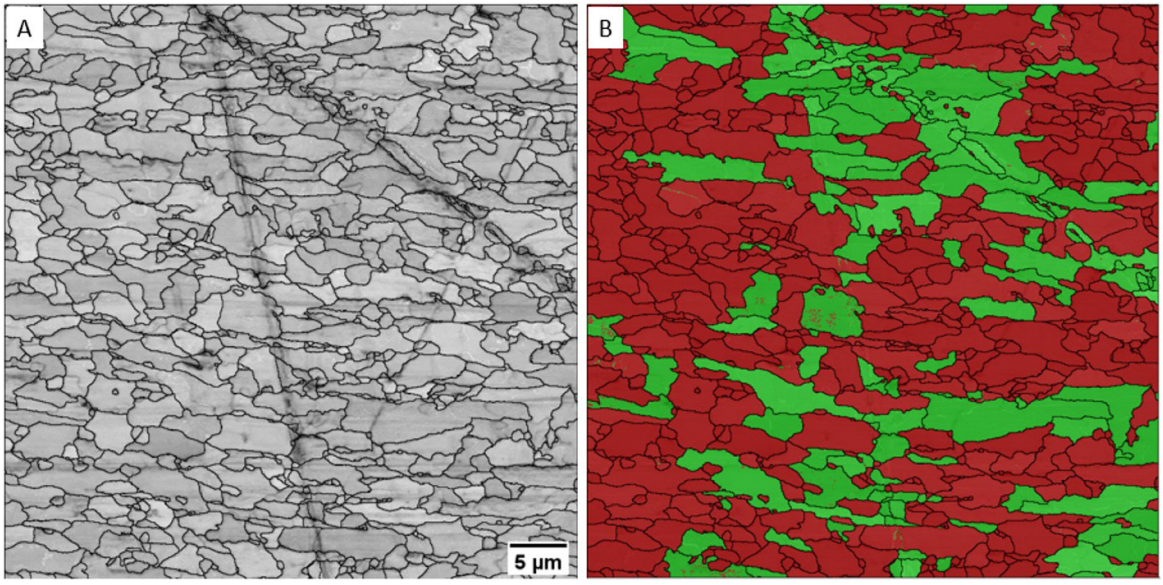

Figure 4. Example of segmentation affected by residual deformation due to sample preparation. A – Band Contrast image showing residual scratches. B – Segmented map with bainite (Green) concentrated in the scratched regions and ferrite (Red).

and blue as austenite. The phases quantification obtained from the EBSD segmentation is presented in Table 4.

The quantification results can be double checked by comparing the LOM and EBSD values. Although martensite and bainite were not distinguished from the LOM images, the ferrite amount showed to be consistent with the EBSD results. The combination of martensite and bainite content are also in agreement with the LOM quantification. In fact, the raw

Table 3. LOM quantification results from the different phases in the CP1100 steel

Steel	Ferrite %	Bainite/Martensite %	Retained Austenite%
CP1100	54 ± 3.7	45.3 ± 3.6	0.78 ± 0.25

Table 4. EBSD quantification results from the different microconstituents in the CP1100 steel and the amount calculated by the proposed method

Steel	Ferrite %	Bainite %	Martensite %	RA %
CP1100 (EBSD)	56.3 ± 4	21.1 ± 4.1	21.2 ± 1.5	1.4 ± 1
CP1100 (Calculated)	*	23.6 ± 1.3	21.6 ±1.3	*

*Value is not calculated.

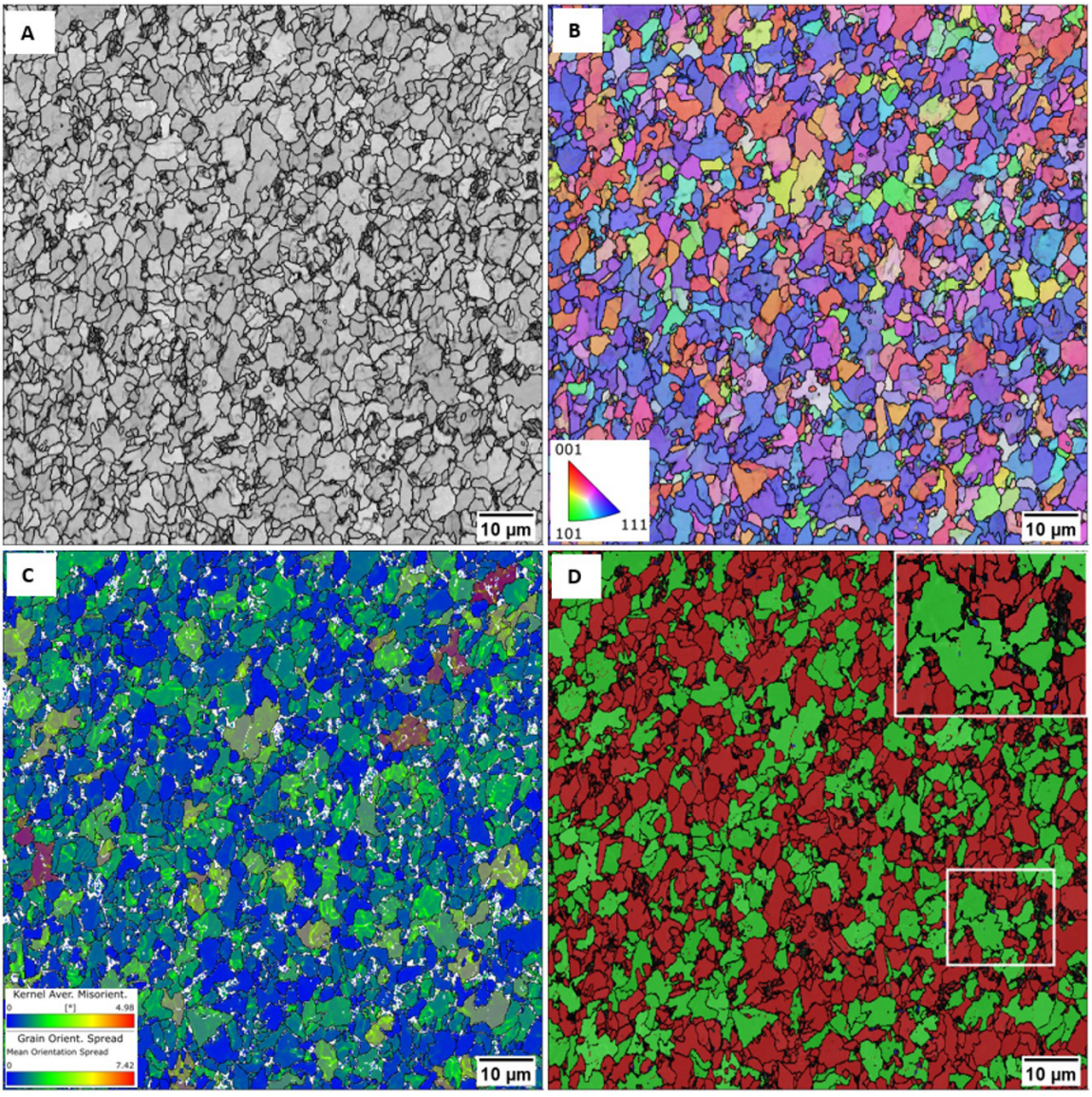

Figure 5. EBSD segmentation of a CP steel. A – BC map. B – IPF map. C – KAM + GOS map. D – Segmented map, where red is ferrite, green is bainite, black is martensite, and blue is retained austenite. Inset in Figure 5D shows a small austenite grain.

EBSD results, that is, the phase map quantification value of BCC phase (combination of ferrite and bainite) can be used to confirm the amount of bainite using the LOM quantification of ferrite, as it has been done in previous work [14]. The following straight calculations can be performed for the microconstituents quantification based in the proposed approach:

$$EBSD_{raw\,BCC} - LOM_{Ferrite} = Bainite_{calculated} \quad (1)$$

$$LOM_{martensite/bainite} - Bainite_{calculated} = Martensite_{calculated} \quad (2)$$

The martensite content measured by both ways can be compared to confirm if the quantification is correct. If inconsistencies are observed, it will be known that some quantification problem occurred during the EBSD analysis.

$$Martensite_{calculated} \approx EBSD_{Martensite} \quad (3)$$

The quantification results presented here were also confirmed using dilatometry and X-ray diffraction analysis, which was published previously [10]. A student t test conducted using six EBSD maps shows a result of 0.18 indication the validity of the method. The best use of this mathematic method is to confirm the EBSD segmentation.

4 Conclusion

A method for phases quantification of the complex-phase steel microstructure using LOM and EBSD analysis was described, and examples were presented. It was also shown that a simple calculation can be done to double check the EBSD quantification. The validity of LOM and EBSD quantification was confirmed.

Acknowledgements

The authors would like to thank the institutions, funding agencies, universities involved in this work: PUC-RIO (Brazil); CSN (Brazil); University of Manchester (UK) ; MINES-ASPPRC (USA); Centro Brasileiro de Pesquisas Físicas (CBPF-Brazil); Instituto Nacional de Tecnologia (INT-Brazil); Coordenação de Aperfeiçoamento de Pessoal de Nível Superior (CAPES-Brazil); Conselho Nacional de Desenvolvimento Científico e Tecnológico (CNPq-Brazil) and the Fundação Carlos Chagas Filho de Amparo à Pesquisa do Estado do Rio de Janeiro (FAPERJ-Brazil).

References

1 Kuziak R, Kawalla R, Waengler S. Advanced high strength steels for automotive industry. Archives of Civil and Mechanical Engineering. 2008 [cited 2022 Sept 13];8(2):103-117. Available at: http://linkinghub.elsevier.com/retrieve/pii/S1644966512601976

2 Karelova A, Krempaszky C, Werner E, Tsipouridis P, Hebesberger T, Pichler A. Hole expansion of dual-phase and complex-phase AHS steels - effect of edge conditions. Steel Research International. 2009;80:71-77.

3 Martin P, Unruh K, Chottin J, Hug E. Damage mechanisms in multiphased a bainitic matrix under various mechanical loading under various mechanical loading paths. Procedia Manufacturing. 2018;15:1557-1564.

4 Vandeputte S, Ruisbroek B, Mesplont C, Lambersart F, Jacobs S, Gent B. Ultra high strength steel composition the process of production of an ultra high strength steel product and the product obtained. Available at: https://image-ppubs.uspto.gov/dirsearch-public/print/downloadPdf/8715427; 2014.

5 Mesplont C. Phase transformations and microstructure - mechanical properties relations in complex phase high strength steels. Local: Universiteit Gent; 2002.

6 Pathak N, Butcher C, Worswick MJ, Bellhouse E, Gao J. Damage evolution in complex-phase and dual-phase steels during edge stretching. Materials (Basel). 2017;10(4):1-29.

7 Sugimoto K, Mukherjee M. TRIP aided and complex phase steels. In: Rana R, Singh SB, editors. Automotive steels: design, metallurgy, processing and applications. Woodhead Publishing: Springer; 2016. p. 217–257. http://dx.doi.org/10.1016/B978-0-08-100638-2.00008-0

8 Hairer F, Karelová A, Krempaszky C, Werner E, Pichler T, Hebesberger A. Etching techniques for the microstructural characterization of complex phase steels by light microscopy. International Doctoral Seminar. 2008 [cited 2022 Sept 13];50-4. Available at: http://www.mtf.stuba.sk/docs/internetovy_casopis/2008/4mimorc/hairer.pdf

9 Hairer F, Krempaszky C, München U. Effects of heat treatment on microstructure and mechanical properties of bainitic single- and complex-phase steel. Materials Science and Technology. 2018;2009:1391-1401.

10 Garcia CI, Hua M, Cho K, DeArdo AJ. New method of characterizing and quantifying complex microstructures in steels. Materials and Manufacturing Processes. 2010;25(1-3):33-40.

11 Kang JY, Kim DH, Baik S II, Ahn TH, Kim YW, Han HN, et al. Phase analysis of steels by grain-averaged EBSD functions. ISIJ International. 2011;51(1):130-136.

12 Li X, Ramazani A, Prahl U, Bleck W. Quantification of complex-phase steel microstructure by using combined EBSD and EPMA measurements. Materials Characterization. 2018;142(May):179-186. http://dx.doi.org/10.1016/j.matchar.2018.05.038.

13 Zhao H, Wynne BP, Palmiere EJ. A phase quantification method based on EBSD data for a continuously cooled microalloyed steel. Materials Characterization. 2017;123:339-348. http://dx.doi.org/10.1016/j.matchar.2016.11.024.

14 Lima RMC, Tolomelli FTS, Clarke AJ, Clarke KD, Spadotto JC, Rizzo FC. Microstructural characterization of A 1100 MPa complex-phase steel. Journal of Materials Research and Technology. 2021;17:184-191.

15 Lima RMC, Spadotto J, Rizzo FC. Use of LOM and EBSD to identify bainite in complex phase steel. Microscopy and Microanalysis. 2021;27(S1):370-372.

16 Tomaz RF, Brandão Santos D, Camey K, Barbosa R, Spangler Andrade M, Pérez Escobar D. Complex phase quantification methodology using electron backscatter diffraction (EBSD) on low manganese high temperature processed steel (HTP) microalloyed steel. Journal of Materials Research and Technology. 2019;8(2):2423-2431. http://dx.doi.org/10.1016/j.jmrt.2019.01.021.

17 Arganda-Carreras I, Kaynig V, Rueden C, Eliceiri KW, Schindelin J, Cardona A, et al. Trainable Weka Segmentation: a machine learning tool for microscopy pixel classification. Bioinformatics (Oxford, England). 2017;33(15):2424-2426.

18 Oxford Instruments. AZtec ® Reclassify Phase: discriminating phases in steels [Internet]. 2016 [cited 2022 Sept 13]. Available at: https://nano.oxinst.com/campaigns/downloads/aztec-reclassify-phase-discriminating-phases-in-steels

19 Nowell MM, Witt RA, True B. EBSD sample preparation: techniques, tips, and tricks. Microscopy and Microanalysis. 2005;11(S02):504-505.

20 Oxford Instruments. Grain size characterisation of a steel sample using the AZtec HKL EBSD system [Internet]. 2022 [cited 2022 Sept 13]. Available at: https://nano.oxinst.com/campaigns/downloads/grain-size-characterisation-of-a-steel-sample-using-the-aztechkl-ebsd-system

21 Oxford Instruments. High resolution EBSD mapping of martensitic steel [Internet]. 2022 [cited 2022 Sept 13]. Available at: https://nano.oxinst.com/campaigns/downloads/high-resolution-ebsd-mapping-of-martensitic-steel

Received: 13 Sept. 2022
Accepted: 12 June 2023